Preparation and Characterization of Poly(ethylene-*co*-vinyl alcohol) Membranes via Thermally Induced Liquid–Liquid Phase Separation

Mengxian Shang,[1] Hideto Matsuyama,[1] Taisuke Maki,[1] Masaaki Teramoto,[1] Douglas R. Lloyd[2]

[1]*Department of Chemistry and Materials Technology, Kyoto Institute of Technology, Matsugasaki, Sakyo-ku, Kyoto 606-8585, Japan*
[2]*Department of Chemical Engineering, University of Texas at Austin, Austin, Texas 78712*

Received 16 October 2001; accepted 12 April 2002

ABSTRACT: Porous membranes were prepared through the thermally induced phase separation of poly(ethylene-*co*-vinyl alcohol) (EVOH)/glycerol mixtures. The binodal temperature and dynamic crystallization temperature were determined by optical microscopy and differential scanning calorimetry measurements, respectively. It was determined experimentally that the liquid–liquid phase boundaries were shifted to higher temperatures when the ethylene content in EVOH increased. For EVOHs with ethylene contents of 32–44 mol %, liquid–liquid phase separation occurred before crystallization. Cellular pores were formed in these membranes. However, only polymer crystallization (solid–liquid phase separation) occurred for EVOH with a 27 mol % ethylene content, and the membrane morphology was the particulate structure. Scanning electron microscopy showed that the sizes of the cellular pores and crystalline particles in the membranes depended on the ethylene content in EVOH, the polymer concentration, and the cooling rate. Furthermore, the tendency of the pore and particle sizes was examined in terms of the solution thermodynamics of the binary mixture and the crystallization kinetics. © 2002 Wiley Periodicals, Inc. J Appl Polym Sci 87: 853–860, 2003

Key words: membranes; phase separation; crystallization; morphology

INTRODUCTION

Poly(ethylene-*co*-vinyl alcohol) (EVOH) is a crystalline random copolymer with hydrophilic vinyl alcohol and hydrophobic ethylene segments. EVOH has been attracting a great deal of attention in biomedical fields because of its insolubility in water and its good blood compatibility. Yamashita et al.,[1] Sakurada et al.,[2] and Chen and Young[3] investigated hemodialysis with EVOH membranes and proved the importance of the EVOH membrane application. It has been asserted in a patent[4] that EVOH membranes have eminent hydrophilicity, superior mechanical properties, and excellent flexibility. In the patent, it is reported that these membranes are suitable for microfilters and battery separators because of their chemical resistance and good permeability and that they can be applied to plasmapheresis because of their good blood compatibility.

Porous EVOH membranes have mainly been prepared by the traditional wet process, that is, the immersion–precipitation method.[5–10] A homogeneous polymer solution is immersed in a nonsolvent bath in this process. The penetration of the nonsolvent into the polymer solution induces phase separation, and a porous structure is consequently formed.

An alternative method for producing porous membranes is thermally induced phase separation (TIPS).[11–19] In the TIPS process, a homogeneous polymer solution melt-blended at a high temperature is cooled to induce phase separation. Therefore, no nonsolvent is required in the TIPS process. In previous articles, we reported porous EVOH membranes prepared by the TIPS process.[20–22] The porous membrane structures were formed by solid–liquid (S–L) phase separation (polymer crystallization) rather than liquid–liquid (L–L) phase separation. The dependency of the crystalline particle size on the polymer concentration, cooling rate, and solvent type was reported.[20] The permeability of EVOH membranes was examined with respect to solutes of various sizes.[21] Higher solute rejection and lower water permeance were obtained with an increase in the polymer concentration in the membrane preparation process and with an increase in the cooling rate in the TIPS process. The effect of the ethylene content (EC) of EVOH on the membrane morphology and solute rejection property was also investigated.[22] Recently, phase diagrams of mixtures of EVOH and poly(ethylene glycol) (PEG) were determined.[23] Both the L–L phase boundaries and the crystallization curves were shifted to higher temperatures when the OH group contents in EVOH

Correspondence to: H. Matsuyama (matuyama@chem.kit.ac.jp).

Journal of Applied Polymer Science, Vol. 87, 853–860 (2003)

TABLE I
Properties of EVOH

Polymer	Ethylene content (mol %)	Crystallization temperature (°C)	Degree of polymerization
EVOH44	44	154.8[a]	940
EVOH38	38	155.1[a]	960
EVOH32	32	165.2[a]	1080
EVOH27	27	165.9[a]	1000

[a] Determined by DSC at the cooling rate of 10 K/min in this work.

increased. However, the membrane structure was not reported in this EVOH/PEG system.

In our previous work, most of the EVOH membranes prepared by the TIPS process were particulate structures.[20–22] In this work, glycerol was used as a diluent to prepare EVOH membranes by L–L phase separation. For the EVOH/glycerol mixtures, L–L phase separation occurred much more easily than S–L phase separation in the TIPS process. However, scanning electron microscopy (SEM) also showed a simultaneous occurrence for both L–L phase separation and crystallization. Furthermore, the effects of the cooling rate and polymer concentration on the pore size of the EVOH membranes were investigated.

EXPERIMENTAL

Materials

Four kinds of EVOHs with different ECs were kindly supplied by Kuraray Co. (Tokyo, Japan). The degrees of polymerization were not very different in the four EVOHs. The properties of the EVOHs are listed in Table I. The numbers following EVOH denote the molar percentage of ethylene. For example, EVOH with 44 mol % ethylene was abbreviated EVOH44. The diluent was glycerol of an extra-pure reagent grade (Wako Pure Chemical Industries, Ltd., Kyoto, Japan). All the materials were used as received without further purification.

Phase diagrams

Homogeneous polymer–diluent samples were prepared by a method reported by Kim and Lloyd.[17] A 3–8-mg sample was sealed in an aluminum differential scanning calorimetry (DSC) pan, melted at 473.2 K for 3 min, and then cooled at two controlled rates of 10 and 100 K/min to 323.2 K with a Perkin Elmer DSC-7. The onset of the exothermic peak during cooling was taken as the dynamic crystallization temperature (T_C).

Cloud points (T_{cloud}'s) were determined with a BX50 optical microscope (Olympus, Tokyo, Japan). The polymer–diluent sample was placed between a pair of microscope coverslips. To prevent diluent loss by evaporation, a 100-μm-thick Teflon film with a square opening in the center was inserted between the coverslips. The coverslip sample was placed on an LK-600 PH hot stage (Linkam, Surrey, UK), heated to 473.2 K for 1 min, and then cooled at a constant rate of 10 K/min to a temperature 5 K above the expected T_{cloud} value with a Linkam L-600A controller. Subsequently, T_{cloud} was determined visually at a cooling rate of 1 K/min from the appearance of turbidity under the microscope.

SEM observations

The coverslips containing the sample were heated on a hot stage at 473.2 K for 2 min, as described previously. The sample was then either immersed in ice water or cooled at a constant rate of 10 or 100 K/min on a hot stage to 298.2 K. The sample was recovered from the coverslips, immersed in water for 1 day for extraction of the diluent, and freeze-dried with an FD-1000 freeze dryer (Tokyo RIKAKIKAI Co., Tokyo, Japan). The microporous membrane was fractured in liquid nitrogen and mounted vertically on a sample holder. The surface of the sample was sputtered with Au/Pd in vacuo. The membrane cross section was viewed with an S-2300 scanning electron microscope (Hitachi Co., Tokyo, Japan).

Pore and particle size measurements

The pore and particle sizes in the SEM photographs were measured with a ruler for the determination of the effect of the polymer concentration and cooling rate on the pore and particle sizes. About 15 pores or particles were measured with random selection for each micrograph, and the measured sizes were averaged. The averaged data obtained by these measurements were taken as the mean pore or particle sizes of the EVOH membranes.

RESULTS AND DISCUSSION

Figure 1 shows the phase diagrams for various EVOHs with different ECs. For EVOHs with ECs of 32–44 mol %, the phase diagrams show upper critical solution temperature (UCST) L–L phase behavior, which reveals that the L–L phase separation occurred before the dynamic crystallization (S–L phase separation) in the lower EVOH concentration. For EVOH with 27 mol % EC (EVOH27), no structure formation was detected with the microscope at a temperature higher than T_C, and T_{cloud}, the border of L–L phase separation, did not exist in the higher temperature region. T_C approximately agreed with the temperature at which particles were detected by the optical microscope during cooling, although the latter is not shown in the figure. Therefore, the EVOH27 membrane structure was formed by S–L phase separation or by crystallization followed by L–L phase separation. These

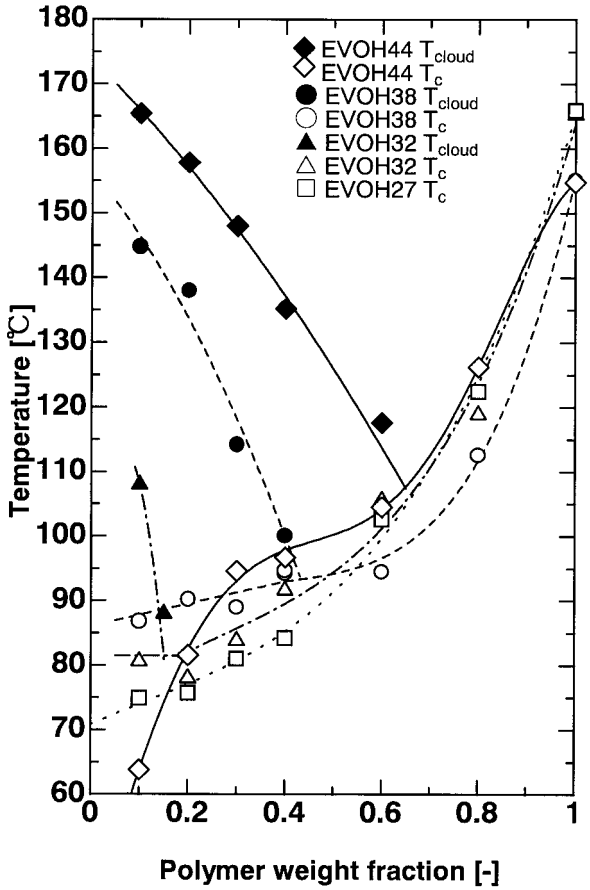

Figure 1 Phase diagram for various EVOHs with different ECs: (—) EVOH44, (–) EVOH38, (– · –) EVOH32, and (· · ·) EVOH27.

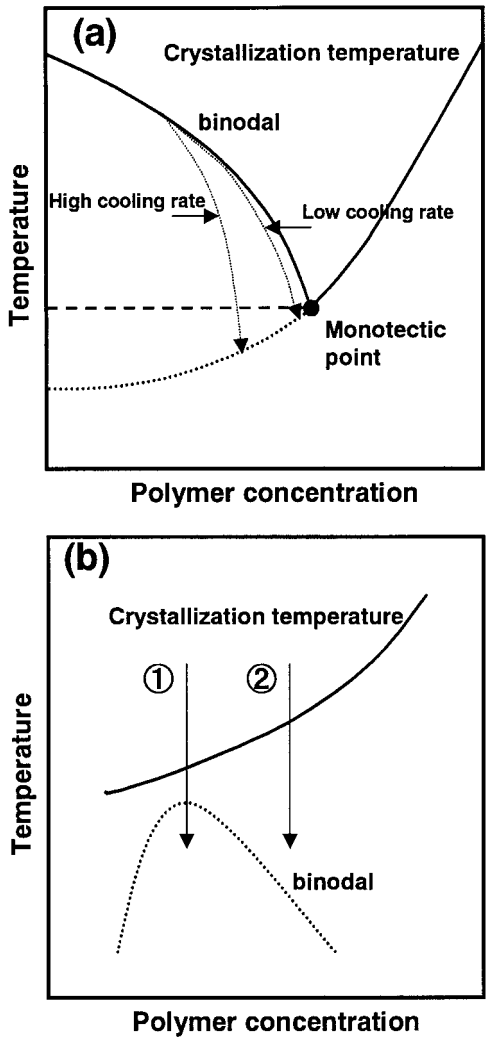

Figure 2 Model phase diagrams and cooling process. (a) Explanation of the result shown in Figure 1, (b) explanation of the result shown in Figure 7.

phase behaviors can be explained by the solubility parameters of these EVOHs and glycerol, which are summarized in Table II.[22] As the EC in EVOH increased, the solubility parameter veered far from the diluent value, and this led to worse compatibility. The worse the compatibility was, the more easily L–L phase separation occurred in the polymer–diluent solution.[23] Therefore, as shown in Figure 1, the L–L phase boundaries were shifted to higher temperatures when the ECs in EVOH increased. The L–L phase boundary was intersected with a crystallization curve at a monotectic point. The polymer concentrations at the monotectic points of EVOH44, EVOH38, and EVOH32 were approximately 63, 42, and 18 wt %, respectively. For EVOH38 and EVOH32, at the polymer concentration lower than the monotectic point, almost horizontal crystallization curves inside the L–L phase region were obtained, and this revealed a behavior typical of L–L phase separation.[24] Moreover, the crystallization temperature in the L–L phase region depended on the monotectic point value. As shown in Figure 1, the higher the EVOH concentration was at the monotectic point, the higher the horizontal crystallization temperature was. For EVOH with 44 mol % EC, however, the crystallization temperature inside the L–L phase region showed a decreasing tendency. From a theoretical point of view, the horizontal crystallization curve could be obtained in the L–L phase region only when the polymer concentrations in the polymer-rich and polymer-poor phases followed the binodal line during cooling. As shown in Figure 1,

TABLE II
Solubility Parameters

Substance	Solubility parameter $[(MPa)^{1/2}]$
Polyethylene	15.76[a]
Poly(vinyl alcohol)	25.78[a]
EVAL27	23.07[b]
EVAL32	22.57[b]
EVAL38	21.97[b]
EVAL44	21.37[b]
Glycerin	33.8[a]

[a] Ref. 25.
[b] Estimated by interpolation from two solubility parameters of polyethylene and poly(vinyl alcohol).[22]

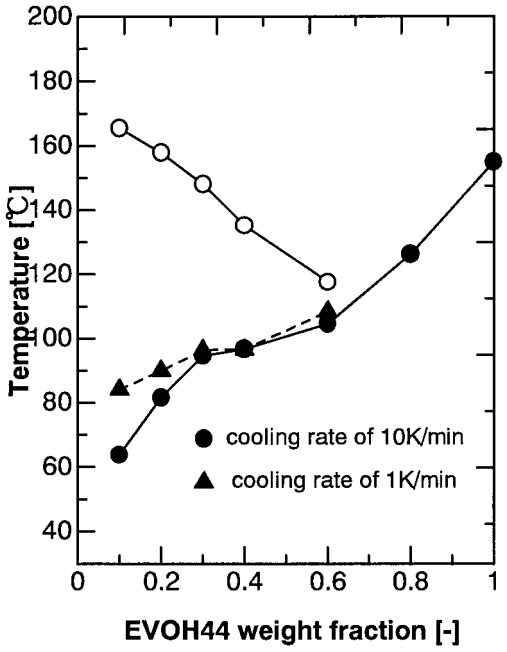

Figure 3 Effect of the cooling rate on T_C in the EVOH44/glycerol systems: (●,▲) T_C and (○) T_{cloud}.

the L–L immiscible region of EVOH44 was very broad, indicating that a considerably long time was required for the polymer concentration to follow the binodal line during cooling. As schematically shown by the dotted line in Figure 2(a), when the cooling rate was lower, the actual concentration of the polymer-rich phase could be closer to the binodal line. This resulted in the T_C value being higher than that at a high cooling rate, although it was still lower than the monotectic point temperature. Therefore, this deviation from the monotectic point temperature shown in Figure 2(a) became smaller with a decreasing cooling rate. In fact, as shown in Figure 3, when the samples were cooled at the rate of 1 K/min, the crystallization curve for the concentration lower than the monotectic point more closely approached the horizontal type than those cooled at the rate of 100 K/min. This agreed with our expectations.

Figure 4 shows the cross sections of the membranes formed at a cooling rate of 10 K/min with various initial polymer concentrations of EVOH38. Because the monotectic point in this system was approximately 42 wt %, as shown in Figure 1, L–L TIPS occurred before crystallization for 10–40 wt %. Therefore, cellular pores derived from L–L phase separation were obtained in all cases, and the pore size decreased with increasing polymer concentration. The spherulite formed by polymer crystallization was observed in the 40 wt % sample. As shown in Figure 1, T_{cloud} of the 40 wt % sample was a littler higher than the crystalliza-

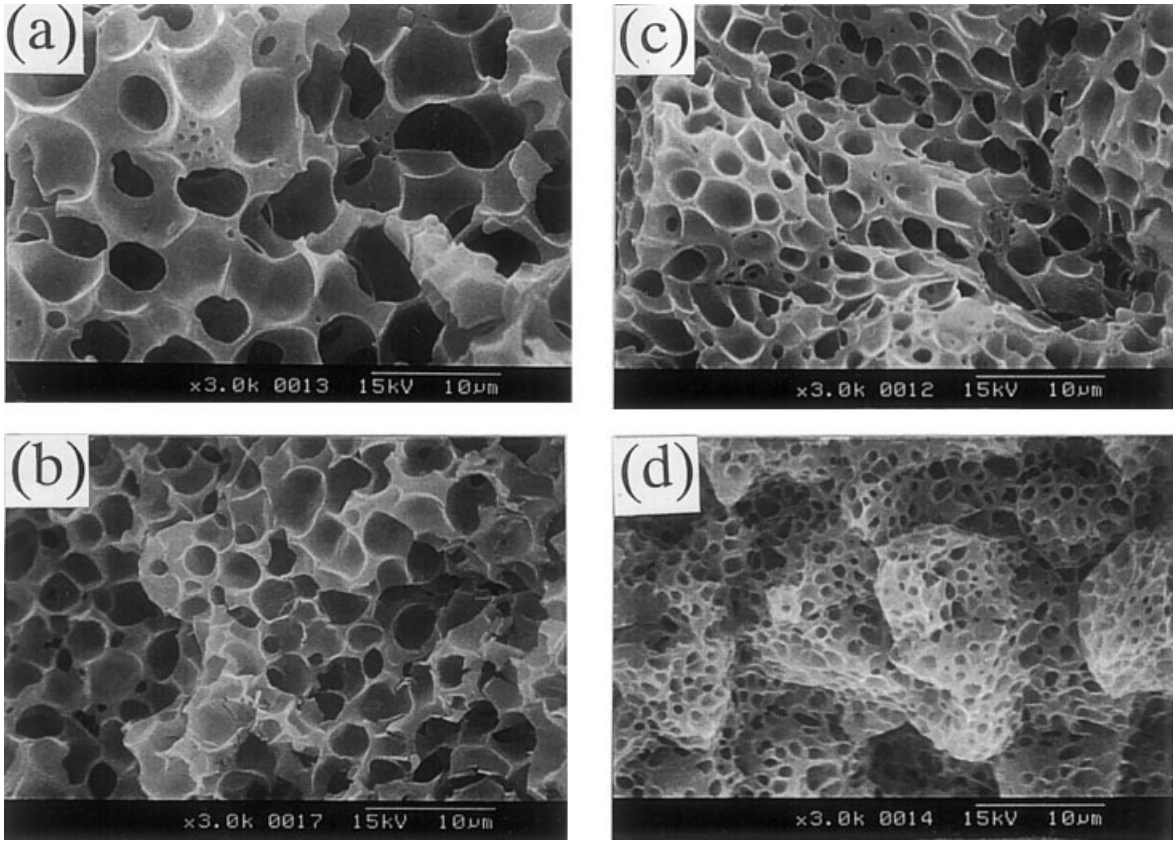

Figure 4 Micrographs of the cross sections of EVOH38 membranes (cooling rate = 10 K/min) with various polymer concentrations: (a) 10, (b) 20, (c) 30, and (d) 40 wt %.

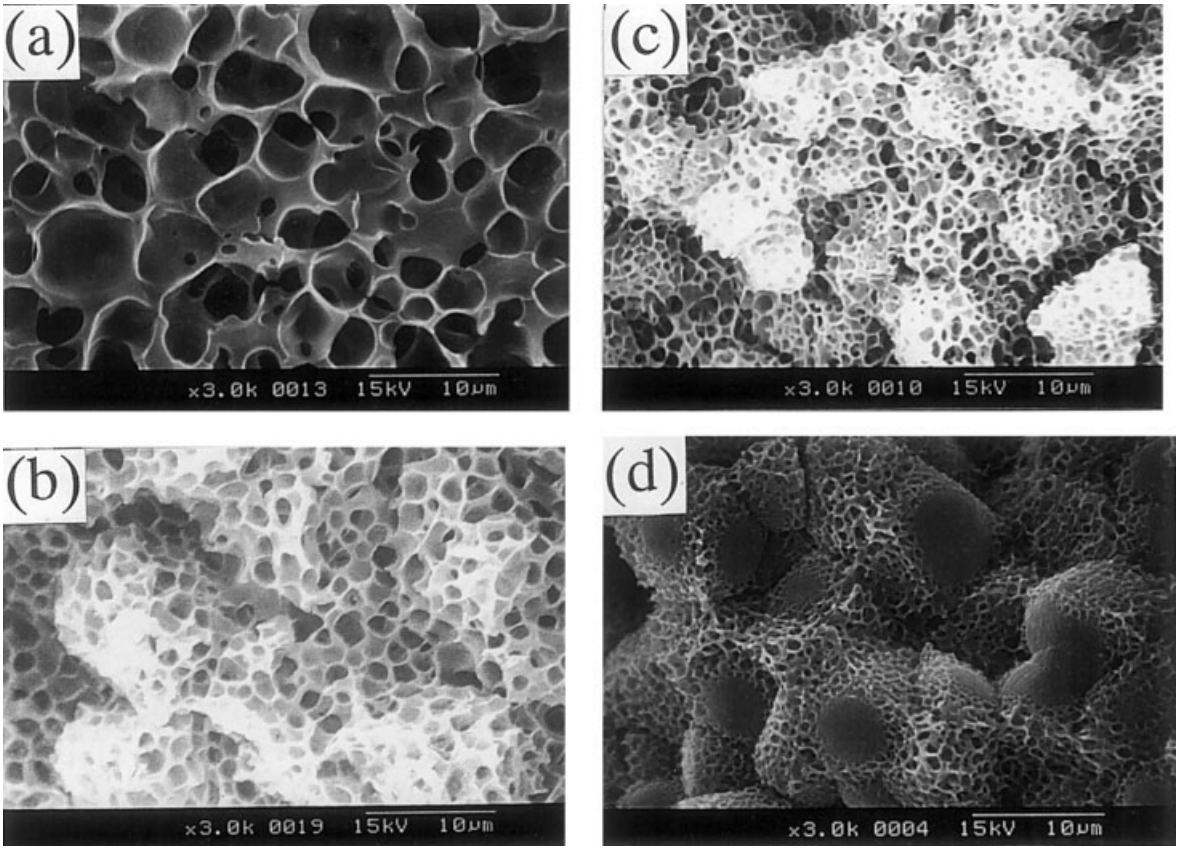

Figure 5 Micrographs of the cross sections of EVOH32 membranes (cooling rate = 10 K/min) with various polymer concentrations: (a) 10, (b) 20, (c) 30, and (d) 40 wt %.

tion temperature. Therefore, polymer crystallization occurred just after the L–L phase separation.

Figure 5 shows the membrane structures with EVOH32. As shown in Figure 1, the monotectic point in this system existed between 10 and 20 wt %. Therefore, only well-connected cellular pores were obtained in the 10 wt % sample. However, both spherulites and cellular pores were obtained in the samples with polymer concentrations of 20–40 wt %. In these cases, the L–L phase separation occurred just after the polymer crystallization. Moreover, the SEM micrographs showed the same decreasing tendency in the pore size with an increasing polymer concentration as shown in Figure 4. The porosity in the 40 wt % sample was smaller than that in the 10, 20, and 30 wt % samples. This can be explained by the smaller volume fraction of the polymer-poor phase in the 40 wt % sample.

Figure 6 shows the cellular pore size of various EVOHs samples cooled at 10 K/min. As described previously, the pore size decreased with an increasing polymer concentration in three EVOH cases. This decrease was due to two factors.[26] First, as the polymer concentration increased, there was less time for coarsening of the polymer-poor phase droplet. The droplet was formed by phase separation when the temperature reached the binodal point and could grow during the cooling until the temperature reached the crystallization temperature. Finally, the membrane structure was solidified by crystallization. As the polymer concentration increased, the region between the binodal

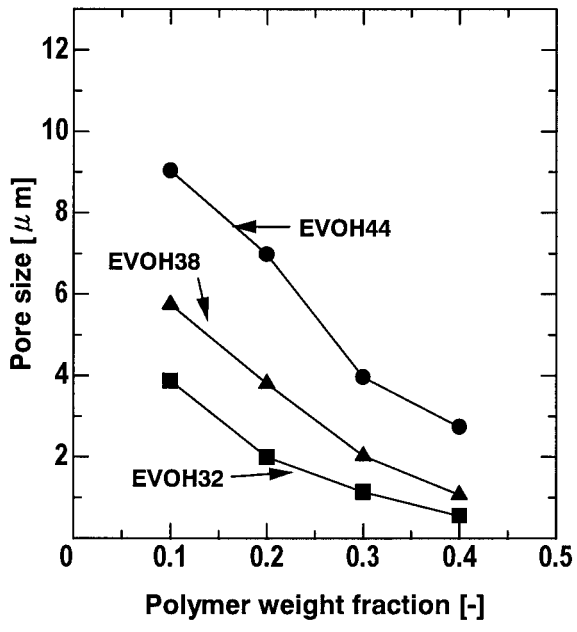

Figure 6 Effect of the polymer concentration on the pore size (cooling rate = 10 K/min).

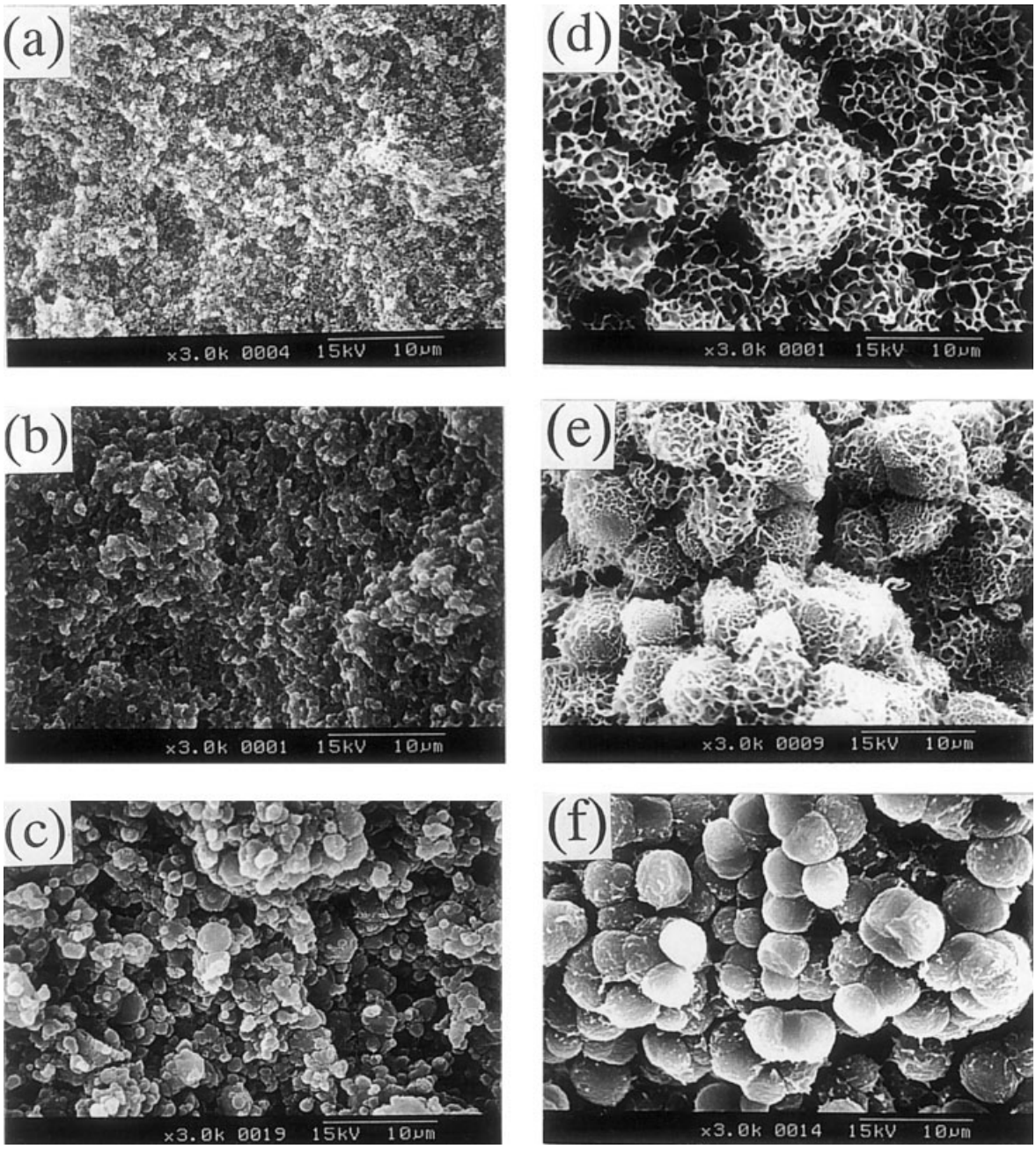

Figure 7 Micrographs of the cross sections of EVOH27 membranes: (a–c) cooling rate = 100 K/min, (d–f) cooling rate = 10 K/min, (a,d) polymer concentration = 20 wt %, (b,e) polymer concentration = 30 wt %, and (c,f) polymer concentration = 40 wt %.

and crystallization temperatures became narrow, as shown in Figure 1. This meant less time for the coarsening. Second, coarsening of the droplets was slower for higher polymer concentrations because of the higher viscosity of the polymer-rich matrix and the smaller volume fraction in the polymer-poor droplet phase. At the same polymer concentrations for these three kinds of EVOHs, the pore size increased with EC increasing from 32 to 44 mol %. This result was attributable mainly to the higher binodal line shown in Figure 1, which led to a longer time for the coarsening of droplets in the polymer samples with higher ECs.

The structures of the EVOH27 membranes cooled at 10 and 100 K/min are shown in Figure 7. When the samples were cooled at a rate of 100 K/min, SEM micrographs showed only the particulate structures, which were typical structures for the polymer crystallization, and no cellular pores were detected because only the crystallization temperature was detected in the EVOH27 case, as shown in Figure 1. However, at the cooling rate of 10 K/min, the 20 and 30 wt % samples showed both the spherulite and cellular pore structures, whereas the 40 wt % sample showed only the particulate structure. This result can be explained

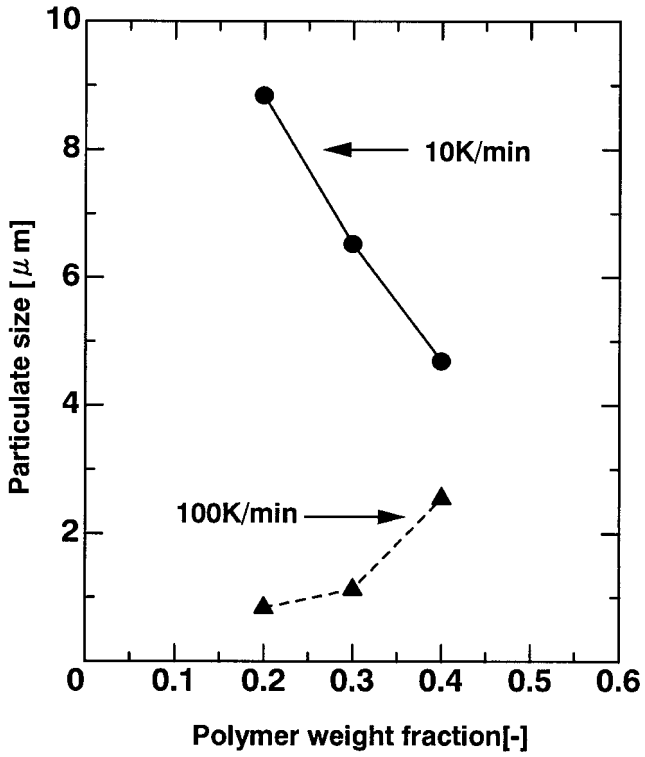

Figure 8 Effect of the cooling rate on the particle size for EVOH27.

by Figure 2(b). In the EVOH27 case, the binodal line existed below the dynamic crystallization curve, and this meant that crystallization occurred before L–L phase separation during cooling. However, for a low cooling rate of 10 K/min, there was more time before structure solidification. Therefore, L–L phase separation could occur in addition to polymer crystallization. As shown by line 1 in Figure 2(b), the binodal line in the low polymer concentration region was close to the crystallization curve, and this meant that L–L phase separation was likely to occur after the crystallization. However, at the higher polymer concentration, shown by line 2, T_{cloud} was much lower than the crystallization temperature, which only led to the occurrence of crystallization until crystalline growth ceased. Therefore, both spherulites and cellular pores were detected in the 20 wt % and 30 wt % samples, and only a particulate structure was detected in the 40 wt % sample in Figure 7.

Figure 8 shows the effect of the cooling rate on the particle size of EVOH27 membranes. When the polymer solutions were cooled at a rate of 100 K/min, the particle size increased with an increasing polymer concentration. As shown in Figure 1, T_C became higher with an increasing EVOH27 concentration. Therefore, for the higher EVOH 27 concentration, the polymer mobility was higher at the beginning of the crystallization because of the high temperature, and the crystallization period from the onset to cessation of the crystallization at the low temperature was longer if the crystallization was stopped at the same temperature for any concentration. This could lead to larger particles because of the higher crystalline growth for the higher EVOH27 concentration. This tendency was the same as that obtained previously.[20] At the same polymer concentration, the samples cooled at the rate of 10 K/min showed larger particles than those cooled at the rate of 100 K/min because of the longer time for spherulite growth. However, for a cooling rate of 10 k/min, the particle size decreased with an increasing concentration of EVOH27, and this was the opposite of the result at the cooling rate of 10 K/min. In this

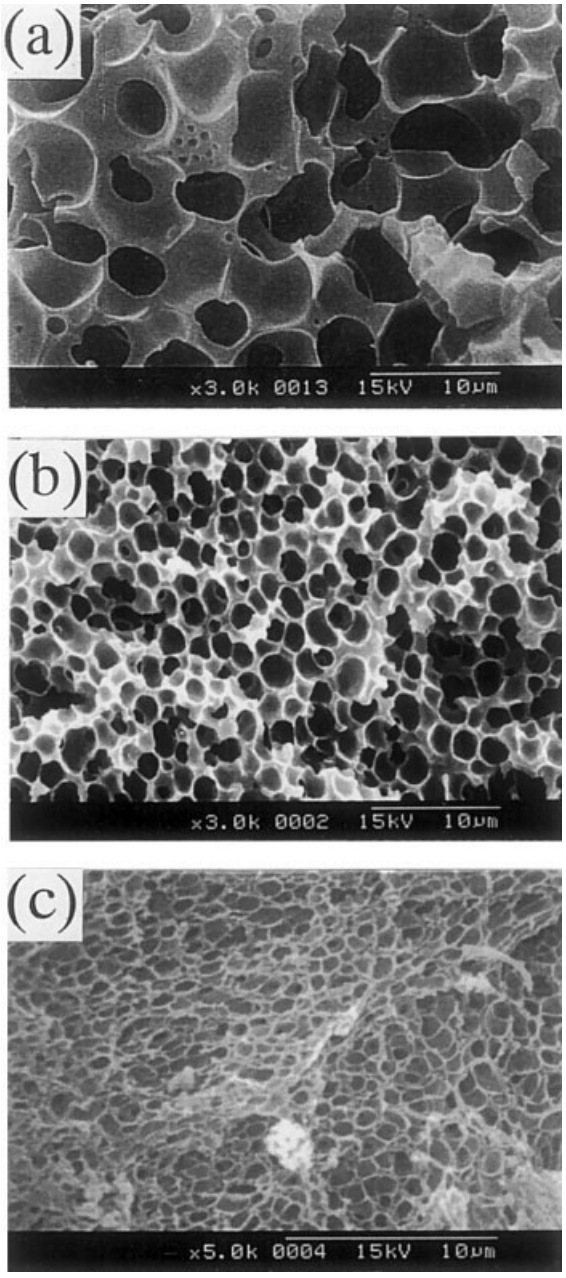

Figure 9 Micrographs of the cross sections of EVOH38 membranes (polymer concentration = 10 wt %): (a) cooling rate = 10 K/min, (b) cooling rate = 100 K/min, and (c) quenched in ice water.

TABLE III
Effect of the Cooling Rate on Pore Sizes for 10 wt % EVOHs

	Pore size of 10 wt % of EVALs (μm)		
Cooling rate (K/min)	EVAL44	EVAL38	EVAL27
10	9.03	5.75	3.87
100	3.94	2.14	1.13
Quenched in ice water	1.23	1.00	0.18

slow-cooling condition, the spherulites could grow and finally contact one another because of the longer time for crystallization. The decrease in the particle size was probably due to the increased spherulite impingement, which resulted from the increased population density of spherulites at the higher polymer concentration.[17]

Figure 9 shows the effect of the cooling rate on the EVOH38 membrane structure. The membrane directly quenched in ice water is also included in this figure. This quenching technique induced faster cooling than 100 K/min. As the cooling rate increased, the pore size decreased, and this tendency agreed with results previously reported.[27]

The effect of the cooling rate on the cellular pore size of 10 wt % EVOH membranes with 44, 38, and 32 mol % ECs is shown in Table III. The pore size decreased with an increasing cooling rate, and this tendency was obtained for all EVOHs. For example, the pore size ranged from 1 to 5.8 μm for EVOH38. The reason for this result is that the droplet coarsening period from T_{cloud} to the structure solidification was longer in the lower cooling rate condition.

CONCLUSIONS

Hydrophilic microporous membranes were prepared from various EVOHs with different ECs. Glycerol was used as a diluent. The phase diagrams of these four polymer–diluent system were determined. For EVOHs with ECs of 32–44 mol %, the T_{cloud} values, which were the border of L–L phase separation, were observed. All phase diagrams in which L–L phase boundaries were observed showed UCST-type phase behavior. When the EC of EVOH increased, the mixture became less compatible, and this shifted the L–L phase boundary and monotectic point to a higher temperature. However, for EVOH with 27 mol % EC, the binodal line existed below the crystallization (S–L phase separation) curve. For the EVOH44–diluent system with a large L–L immiscible region, when the concentration was lower than the monotectic point value, T_C was influenced by the cooling rate. The lower the cooling rate was, the more horizontal the dynamic crystallization curve became.

The effects of the initial polymer concentration and cooling rate on the membrane structures were investigated. Well-connected cellular pore structures were obtained when the initial polymer concentration was lower than the monotectic point value. The pore size decreased with increases in both the polymer concentration and the cooling rate. For EVOH with a 27 mol % EC, polymer crystallization occurred before L–L phase separation during the cooling. At the low cooling rate, the particle size decreased with the increase in the polymer concentration, whereas the opposite tendency was obtained at the high cooling rate.

References

1. Yamashita, S.; Nagata, S.; Takakura, K. Kobunshi Ronbunshu 1979, 36, 249.
2. Sakurada, Y.; Sueoka, A.; Kawahashi, M. Polym J 1987, 19, 501.
3. Chen, L.-W.; Young, T. H. Makromol Chem Macromol Symp 1990, 33, 183.
4. Doi, Y.; Matsuda, K.; Kono, M. Jpn. Pat. 1-3A505 (1989).
5. Matsumoto, T.; Nakamae, K.; Ochiumi, T.; Horie, S. J Membr Sci 1981, 9, 109.
6. Young, T.-H.; Lai, J.-Y.; You, W.-M.; Cheng, L.-P. J Membr Sci 1997, 128, 55.
7. Cheng, L.-P.; Young, T.-H.; You, W.-M. J Membr Sci 1998, 145, 77.
8. Young, T.-H.; Hsieh, C.-C.; Chen, L.-Y.; Huang, Y.-S. J Membr Sci 1999, 159, 21.
9. Young, T.-H.; Huang, Y.-H.; Chen, L.-Y. J Membr Sci 2000, 164, 111.
10. Cheng, L.-P.; Lin, H.-Y.; Chen, L.-W.; Young, T.-H. Polymer 1998, 39, 2135.
11. Castro, A. J. U.S. Pat. 4,247,498, 1981.
12. Caneba, G. T.; Soong, D. S. Macromolecules 1985, 18, 2538.
13. Hiatt, W. C.; Vitzthum, G. H.; Wagener, K. B.; Gerlach, K.; Josefiak, C. In Microporous Membranes via Upper Critical Temperature Phase Separation; Lloyd, D. R., Ed.; ACS Symposium Series 269; American Chemical Society: Washington, DC, 1985; p 229.
14. Lloyd, D. R.; Kinzer, K. E.; Tseng, H. S. J Membr Sci 1990, 52, 239.
15. Tsai, F.-J.; Torkelson, J. M. Macromolecules 1990, 23, 775.
16. Lloyd, D. R.; Kim, S.-S.; Kinzer, K. E. J Membr Sci 1991, 64, 1.
17. Kim, S.-S.; Lloyd, D. R. J Membr Sci 1991, 64, 13.
18. Vadalia, H. C.; Lee, H. K.; Myerson, A. S.; Levon, K. J Membr Sci 1994, 89, 37.
19. Mehta, R. H.; Madsen, D. A.; Kalika, D. S. J Membr Sci 1995, 107, 93.
20. Matsuyama, H.; Iwatani, T.; Kitamaru, Y.; Teramoto, M.; Sugo, N. J Appl Polym Sci 2001, 79, 2449.
21. Matsuyama, H.; Iwatani, T.; Kitamaru, Y.; Teramoto, M.; Sugo, N. J Appl Polym Sci 2001, 79, 2456.
22. Matsuyama, H.; Kobayashi, K.; Maki, T.; Teramoto, M.; Tsuruta, H. J Appl Polym Sci 2001, 82, 2583.
23. Liu, B.; Du, Q.-G.; Yang, Y.-L. J Membr Sci 2000, 180, 81.
24. Burghardt, W. R. Macromolecules 1989, 22, 2482.
25. Brandrop, J.; Immergut, E. H. Polymer Parameters Handbook, 3rd ed.; Wiley: New York, 1989.
26. Matsuyama, H.; Yuasa, M.; Kitamura, Y.; Teramoto, M.; Lloyd, D. R. J Membr Sci 2000, 179, 91.
27. Matsuyama, H.; Berghmans, S.; Lloyd, D. R. J Membr Sci 1998, 142, 21.